Spectral Variability of the Peculiar A-Type Supergiant 3 Pup

By: E. L. Chentsov, V. G. Klochkova, and A. S. Miroshnichenko

Chentsov, E. L., Klochkova, V. G., and Miroshnichenko, A. S. 2010. Spectral Variability of the Peculiar A-Type Supergiant 3 Pup. *Astrophysical Bulletin*, 65(2), 159-172

Abstract:
Optical spectra taken in 1997–2008 are used to analyze the spectral peculiarities and velocity field in the atmosphere of the peculiar supergiant 3 Pup. The profiles of strong Fe II lines and of the lines of other iron-group ions have a specific shape: the wings are raised by emissions, whereas the core is sharpened by a depression. The latter feature becomes more pronounced with the increasing line strength, and the increasing wavelength. Line profiles are variable: the magnitude and sign of the absorption asymmetry, and the blue-to-red emission intensity ratios vary from one spectrum to another. The temporal V_r variations are minimal for the forbidden emissions and sharp shell cores of the absorption features of Fe II(42), and other strong lines of iron-group ions. The average velocity for the above lines can be adopted as the systemic velocity: $V_{sys} = 28.5 \pm 0.5$ km/s. The weakest photospheric absorptions and photospheric Mg II, Si II absorptions exhibit well-defined day-to-day velocity variations of up to 7 km/s. Quantitative spectral classification yields the spectral type of A2.7±0.3 Ib. The equivalent widths and profiles of Hδ and Hγ, and the equivalent width of the OI7774 Å triplet yield an absolute magnitude estimate of $Mv = -5.5^m \pm 0.3^m$, implying the heliocentric distance of 0.7 kpc.
Key words: stars—variable and peculiar

Article:

1. INTRODUCTION

The nature of the bright star 3 Pup (HD 62623 = HR 2996 = MWC 570 = HIP 37677) has long remained unclear. In the Bright Star Catalog [1] this star is listed as a A2 Iabe-type super-giant. However, 3 Pup was also viewed as an object related to stars evolving towards planetary nebulae with binary core [2]. The spectroscopic study of Plets et al. [3], who found the star's atmosphere to have a close-to-solar chemical composition, provided new evidence for the massive supergiant nature of 3 Pup. However, the star has a property that is uncharacteristic to massive A-type supergiants: a circumstellar dust shell. The shell shows up primarily in the form of IR excess (3 Pup was identified with the IR source IRAS 07418−2850) and specific two-peaked emission features in the optical spectrum.

The star's magnitudes are $B = 4.12^m$ and $V = 3.98^m$, and the color excess $E(B–V) = 0.08^m$ [4]. Its Galactic and equatorial J2000 coordinates are $l = 244.4°$, $b = -2.5°$ and $\alpha = 07^h43^m48^s$, $\delta = -28°57'17''$,respectively. The recently refined parallax [5] is $\pi = 0.59 \pm 0.17''$. Because of its high brightness 3 Pup was chosen as one of the several hundred stars used as the basis of Harvard spectral classification. However, whereas Cannon [6] assigned to it the same spectral type A2 pec as to α Cyg (the peculiarity of both stars showed up in the form of too narrow and weak hydrogen lines, i.e., both stars are supergiants), Maury [7] noticed that 3 Pup has a somewhat lower temperature and luminosity than α Cyg, A2–A3 and Ib–II, respectively, in the currently adopted notation.

Merrill [8] found several emission lines in the spectrum of 3 Pup: a double Hα line with a relatively stronger red component (a P Cyg III type profile according to Beals [9]), [OI] 1F 6300, 6364 Å, FeII(40) 6433, 6516 Å. He also suspected the presence of emission features in some other FeII lines. Emission features in the profiles of

Hβ, Hγ [10] and NaI(1) doublet [3] were noticed only 60 years later. The known infrared emission features include the strong CaII (2) 8498, 8542, 8562 Å triplet [11], and the [CaII]1F 7291, 7324 Å doublet [12] (these lines were erroneously attributed to [OII]). As for absorption lines, the eye estimates of their intensities in the 3120–6565 Å wavelength interval [13, 14] confirmed a lower excitation temperature of 3 Pup, compared to that of α Cyg, as it followed from the classification of Maury, and revealed shell signatures in the star's spectrum. In particular, the MgII (4) and SiII (1,2,3) absorptions in the spectrum of 3 Pup are weaker than the same absorptions in the spectrum of α Cyg, whereas the FeII (42) lines are enhanced compared to FeII (37, 38, 49) lines. The differences between the spectra of a supergiant and a shell star are readily seen in Plate 22 in the atlas of Morgan et al. [15], where they are illustrated on the examples of α Cyg (A2 Ia) and 17 Lep (Ap sh). The temperature of 3 Pup is close to the temperatures of both stars, but its spectrum is closer to that of 17 Lep by a number of features (the depth of TiII and FeII lines and the widths of hydrogen lines).

Table 1. Log of the spectra of 3 Pup used in this paper. The last column gives some details concerning the telluric-line correction of V_r.

Date	Δλ	Spectrograph	λ/Δλ	Remarks
12.11.97	4690–8600	PFES	15000	for λ >5800 Å
3.12.98	3940–5675	PFES	15000	-
14.03.03	5160–6650	NES	60000	with errors of about 0.2 km/s
25.12.04	3700–8870	CFHT	70000	with errors of about 0.2 km/s
26.12.06	3650–8600	McDon	60000	with errors of about 0.2 km/s
7.02.07	4550–6010	NES	60000	with errors of about 0.2 km/s
4.11.08	4460–5930	NES	60000	with errors of about 0.2 km/s

It became clear from the very first inspection of the available spectra of 3 Pup that it must be a very promising object for high-resolution spectroscopy: the star is bright and its spectrum abounds in various, mostly weak, but well-defined features. But however strange it may appear, its optical and near-infrared spectrum has not yet been thoroughly described. This circumstance led us to include 3 Pup into our list of program stars with circumstellar shells for a detailed spectroscopic analysis and repeated observations in order to study the expected spectral variability.

2. OBSERVATIONS AND REDUCTION OF SPECTRA

We obtained the spectra of 3 Pup with the NES echelle spectrograph mounted at the Nasmyth focus of the 6-m telescope of the Special Astrophysical Observatory of the Russian Academy of Sciences (SAO RAS) [16, 17]. Observations were made with a 2048 × 2048 CCD and an image slicer [17]. The spectroscopic resolution and the signal-to-noise ratio are $\lambda/\Delta\lambda \geq 60000$ and S/N≥ 100, respectively. To extend the time interval of observations of 3 Pup, we use the intermediate-resolution spectra that we took in 1997–1998 in the prime focus of the 6-m telescope with the PFES echelle spectrograph [18]. We used a modified ECHELLE context [19] of the MIDAS package to extract one-dimensional vectors from the two-dimensional echelle spectra. Cosmic-ray hits were removed via median averaging of two successively taken spectra. Wavelength calibration was performed using the spectra of a hollow-cathode Th–Ar lamp.

In addition to the spectra taken with the NE S spectrograph, we used high-resolution spectra of the star taken with the ESPaDOnS spectrograph [20] of the 4-m CFHT telescope, and the cs23 spectrograph [21] operating in the coude focus of the 2.7- m telescope of the McDonald observatory. The latter spectra were reduced using the IRAF software package. Table 1 lists the dates of all observations, recorded regions of the spectrum, the spectrographs employed, and the spectral resolution. Table 2 lists the inferred heliocentric radial velocities V_r.

We used the telluric [OI], O_2, and H_2O lines to control and correct the instrumental matching of the spectra of the star and the hollow-cathode lamp. The last column of Table 1 indicates whether a correction has been applied, and the residual errors for each spectrum. For a more detailed description of the procedure of radial velocity V_r measurement from the spectra taken with the NES spectrograph, and the sources of errors, see [22].

The r.m.s. error of the measured V_r for stars with narrow absorption lines in the spectrum is less than 0.8 km/s (the accuracy of the velocity inferred from a single line).

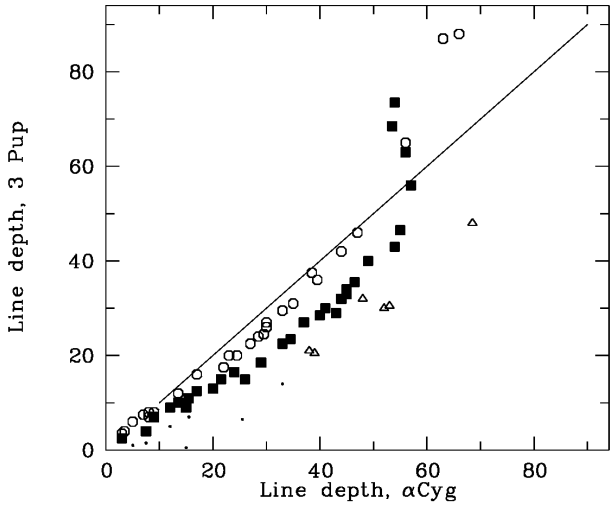

Fig. 1. Comparison of the central line depths R in the spectra of 3 Pup (the vertical axis) and α Cyg (the horizontal axis). The open circles correspond to Ti II lines in the 3680–5190 Å wavelength interval; the filled squares, to the Fe II lines in the 3780–5170 Å wavelength interval; the dots, to the Fe II lines in the 5990–6520 Å wavelength interval, and the triangles, to the MgII (4) and SiII (1,2,3) lines.

3. DISCUSSION OF THE RESULTS

3.1. Peculiarity of the Optical Spectrum of 3 Pup

A comparison of the line profiles and parameters in our spectra of 3 Pup, and in the spectra of the comparison stars obtained with the same spectral resolution showed that the shell appears not solely in the form of several lines mentioned above. The shell signature grows gradually—both with the line intensity and line wavelength. Figure 1 compares the central depths of absorption lines in the spectra of 3 Pup and α Cyg (the depth corresponding to zero residual intensity is assumed to be equal to 100). Whereas Mg II and Si II lines at any intensities and in any part of the optical spectrum are deeper for α Cyg than for 3 Pup, the Ti II and Fe II lines of low and intermediate intensity located in the blue part of the spectrum are deeper for α Cyg, but with the increasing intensity, the depths of these lines in the spectra of the two stars become closer to each other and the strongest TiII (13) and FeII (42) lines in the spectrum of 3 Pup are deeper than the corresponding lines in the spectrum of α Cyg. In the yellow part of the spectrum of 3 Pup, Fe II absorptions are anomalously weak (the bottom left corner of Fig. 1), they are all to a certain extent "raised" by emissions, in some of them the absorption core of the profile is uplifted to the continuum level. Note that in this case the Mg II and SiII absorptions in the spectrum of 3 Pup are weaker than the corresponding absorptions in the spectrum of α Cyg both in terms of depths and equivalent widths (which in the case of Mg II 4481 are equal to 0.56 and 0.66Å, respectively), and the equivalent widths of the TiII (13) doublet are approximately the same in the spectra of both stars. As it is evident from Fig. 2, the smaller widths of these lines in the spectra of 3 Pup are compensated by their greater depth. The profiles of the TiII (13) and FeII (42) lines have the same shape. In Fig. 3 we compare the profiles of FeII lines of different intensity in the spectra of 3 Pup and α Cyg and with the profiles of the MgII 4481 line. In α Cyg all lines form near the photosphere, they are symmetric and differ only in depth. The only true photospheric line in the spectrum of 3 Pup is MgII 4481 Å, whereas FeII features exhibit evident contribution of the shell, which gives the profiles their specific shape: the wings are raised by emissions, whereas the line core is sharpened. The latter shows up even for absorptions with depths $R \approx 20$ and becomes stronger with increasing line strength, thereby explaining the upward bends of the symbol chains in Fig. 1. Pointed cores are also typical for Hβ–H8 Balmer lines, their central depths are smaller than the corresponding central depths in the spectra of a Cyg.

Emissions in the wings become apparent in high-resolution spectra starting at least from $\lambda \approx 4300$ Å. Figure 4 illustrates the variation of the line profile with wavelength: as we move from the blue part of the spectrum towards its red part, the absorptions gradually give way to the two-peaked emissions with an intensity gap at the

center. The profile of the double emission of FeII (40) 6433 Å (the upper profile in Fig. 4) repeats in Fig. 5, as compared to the profiles of the CaII (2) 8542 Å permitted line and several forbidden lines. In the spectrum of 3 Pup the latter are represented not only by the [OI] 1F and [CaII]1 F doublets mentioned above, but also by numerous weak [FeII] lines.

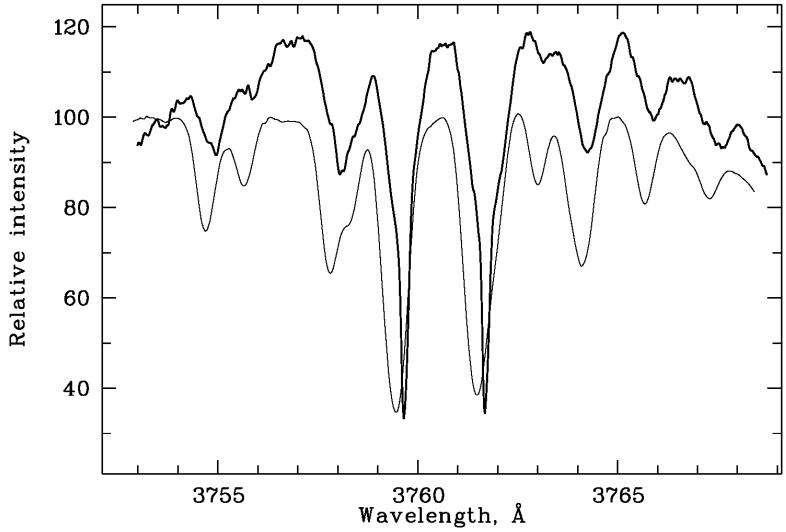

Fig. 2. Spectra of α Cyg (the thin line at the bottom) and 3 Pup (shifted upward by 20 scale points). The strongest lines are TiII (13) 3759 and 3761 Å. The spectrum of 3 Pup at the borders of the figure is depressed by the wings of the H12 3750 and H11 3771 Å lines. Here and in the subsequent figures the relative intensity $r = 100$ corresponds to the continuum level.

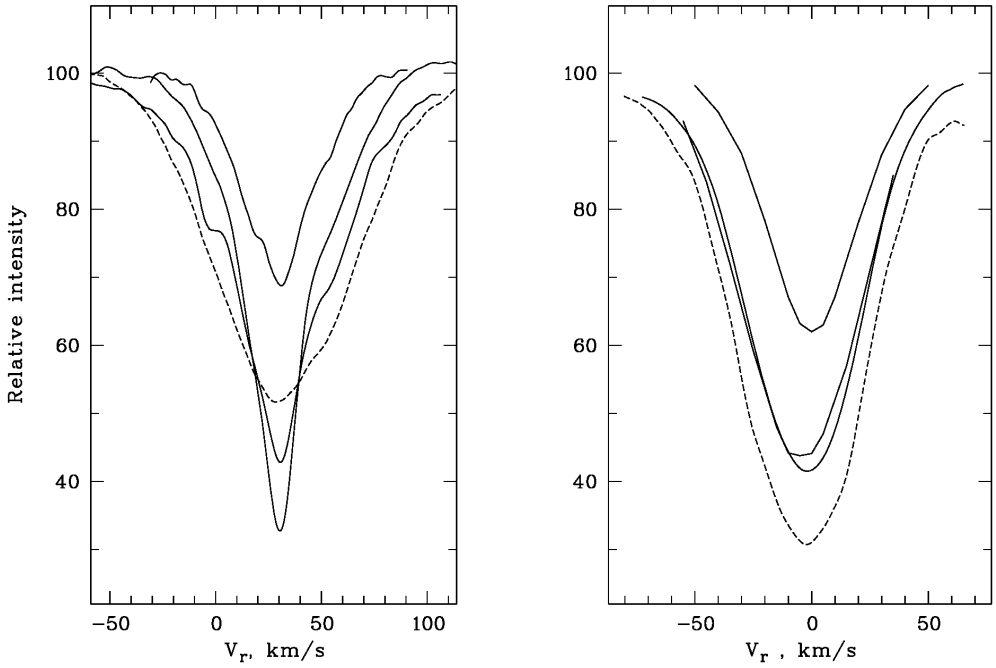

Fig. 3. Profiles of the Fe II and MgII (4) lines in the spectra of 3 Pup (December 26, 2006, on the left) and α Cyg (on the right). The solid lines (from top to bottom) show the profiles of the following lines: FeII (49) 5235 Å, FeII (27) 4233 Å, and FeII (42) 4924 Å. The dashed lines show the profiles of MgII 4481 Å.

A comparison of the emission profiles provides important information about the geometry and kinematics of the 3 Pup shell. All forbidden emissions in the accessible region of the spectrum have equally shaped profiles with the same widths, and yield the same radial velocity within the errors. Permitted emissions differ from forbidden emissions by greater intensity gradients in the central parts of the profiles, they are appreciably broader (for [OI] 6300 Å and FeII 6433 Å the full widths at the continuum level are equal to 120 and 140 km/s, respectively) and are often systematically offset with respect to forbidden emissions (by 4 km/s on December 25, 2004). The strong forbidden CaII (2) triplet has rather interesting “two-step” profiles (in Fig.5 it is represented by the emission at 8542 Å): the narrow double peak is appreciably shifted redward relative to the broader “pedestal”.

The radial velocity of the peak is close to the velocities of forbidden emissions, whereas that of the lower component of the profile, to the velocities inferred from permitted emissions.

Table 2. Heliocentric velocities inferred from individual lines and the mean velocities averaged over groups of lines in the spectra of 3 Pup. For the NaI and FeII(42) lines observed on December 25, 2004 we list the velocities of the decoupled core components under the corresponding the mean velocities V_r.

	V_r, km/s					
Dates	12.11.97	14.03.03	25.12.04	26.12.06	07.02.07	04.11.08
Interstellar lines:						
NaI(1)	33.2	33.0	33.6	33.3	33.5	33.0
	–	29.6	29.4	29.7	30.6:	30.7:
	–	36.3	37.4	37.4	36.5	35.8
KI(1)	28:	–	28	28.7:	–	–
	–	–	37	–	–	–
CaII(1)	–	–	27.0	28.1	–	–
			38:	–	–	–
DIB	30.5	31:	31.0	29.5	31	29
Stellar emission lines:						
[OI]	31:	27	28	29	–	–
[FeII], [CaII]	25:	–	28	28	30:	26:
FeII etc.	28:	26	24	27.5	28	27
Stellar absorption lines:						
FeII(42)	30	30:	30.5	29.8	29.4	27.3
			28.8			
FeII, TiII, etc.	29.5:	29.5:	28.5	30.5	30.0	28.0
MgII, SiII	27:	32	24	30.2	32:	30
The weakest lines ($r \to 100$)	28	28	23	30.5	29.8	29.2
Hδ	–	–	28	29	–	–
Hγ	–	–	28	26	–	–
Hβ	28	–	28	25	27	26
Hα	24	26	22	26	–	–

Line profiles vary with time. The most evident spectrum-to-spectrum variations are those of the magnitude and sign of the asymmetry of absorptions and the blue-to-red emission intensity ratios. Figure 6 shows these variations for the case of FeII lines and the D 1 NaI (1) line. The latter is less blended with atmospheric water absorptions than D2 line, and its interstellar component shows a better outlined two-component core. The stellar and interstellar components are easy to separate because of the variability of the former. The differences between the profiles disappear at the residual intensity of $r \approx 85$. Above this level we observe the stellar NaI line, the shape of its profile and its evolution with time resemble what we see for the FeII 5363 Å line; below this level we observe the interstellar line, which, unlike what we see in the case of FeII (42) lines, has almost vertical and stable slopes, they merge in the $85 > r > 15$ interval.

3.2. Radial Velocity Variations

The anomalies of line profiles in the spectrum of 3 Pup affect the inferred radial velocities, which depend on the features and methods used to measure them, thereby making it difficult to compare our data with the published results of other authors.

The Lick spectrograms of 1908–24 used by Johnson and Neubauer [23] to classify 3 Pup as a small-amplitude spectroscopic binary were obtained on a blue-sensitive emulsion with an average dispersion

of about 20 Å/mm and were measured visually. The inferred velocities appear to refer to the region of the profiles of relatively strong lines with maximal photographic density gradients. The proposed orbital elements ($P = 137.767^d$, $K = 3.6$ km/s, $\gamma = 25.4$ km/s) have been reproduced for more than 60 years in the catalogs of spectroscopic binaries including the most recent such catalog [24]. Swings [13] used panchromatic plates and found no velocity variations with time or from one group of lines to another. He inferred a mean radial velocity of $V_r \approx 31$ km/s. According to Crespin and Swensson [14], $V_r \approx 27$ km/s.

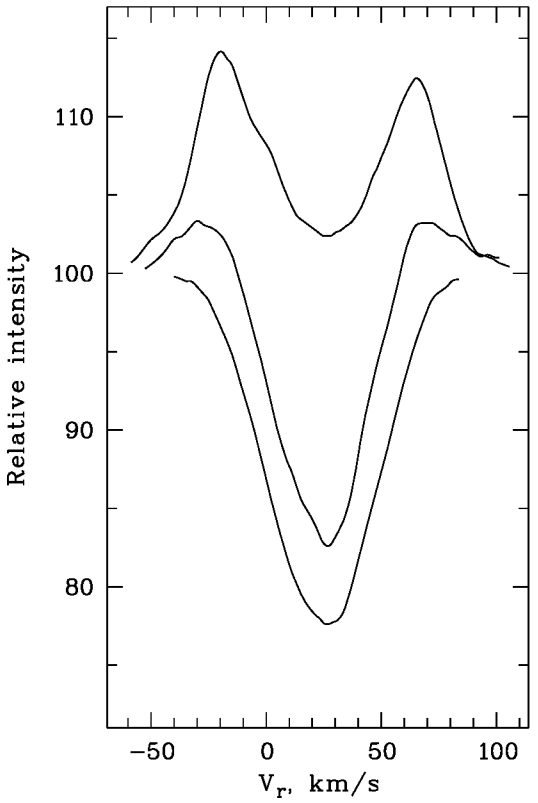

Fig. 4. Evolution of the FeII line profile with wavelength in the spectrum of 3 Pup taken on December 25, 2004. From top to bottom: FeII (28) 4297, FeII (48) 5363, FeII (40) 6433 Å.

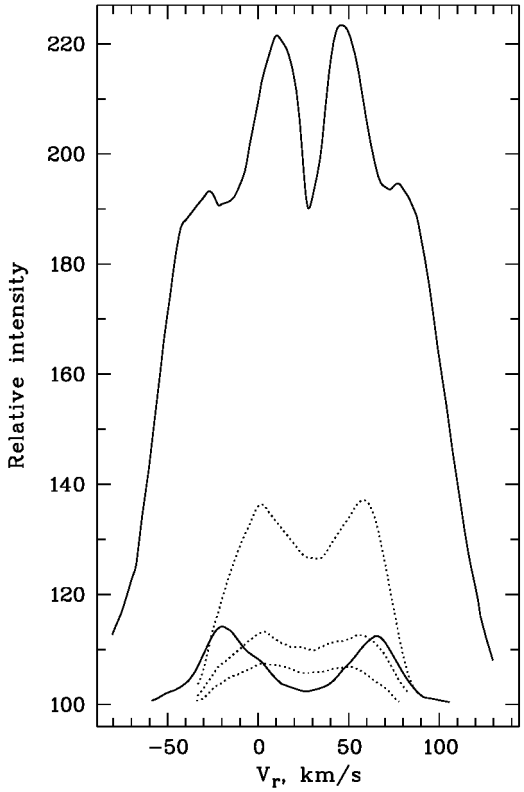

Fig. 5. Non-hydrogen emission features in the spectrum of 3 Pup taken on December 25, 2004. The solid lines show the profiles of permitted lines (from top to bottom) CaII (2) 8542 and FeII (40) 6433 Å. The dashed lines (from top to bottom) show the profiles of the forbidden emissions [CaII]1F 7324, [OI]1F 6300, and [FeII]14F 7155 Å.

In addition, several radial velocity of 3 Pup have been published that were measured from high-resolution (up to 100 000) spectra, but, unfortunately, the authors did not mention the measurement method. Loden [25] used CCD echelle spectra taken during five successive nights in February, 1991. He used 80 lines in the wavelength interval 3850–4870 Å to infer an average radial velocity of $V_r = 28.7$ f 0.2 km/s (in their more recent paper Loden and Sundman [26] corrected slightly this result: 29.3± 1.0 km/s). Plets et al. [3] also had five CCD spectra at their disposal, which were taken from 1986 through 1991 in small, 30–50 Å wide, spectral regions between 3920 and 6180 Å with 5 to 10 lines in each region. The data for four of the five dates yield velocities that range from 27.7 to 30.9 km/s, i.e., are close to the result obtained by Loden [25]. However, the above authors draw different conclusions. Loden [25] found neither the variation of velocity with time nor differential line shifts beyond the measurement errors. Plets et al. [3] combined the new V_r value with some of Johnson and Neubauer data [23] to corroborate the spectroscopic binarity of 3 Pup.

We performed our radial velocity measurements via a mutual wavelength shift so as to align the direct and reversed images of the line profile. In this way, we can determine the velocities of individual features of the line profile. The list of lines used to measure the velocities can be found in Table 3. The complete electronic version of this table is available at www.sao.ru/hq/ssl/3Pup-lines.ps and www.sao.ru/hq/ssl/3Pup/Table3.html. It

contains the results of identification of the features; the adopted laboratory wavelengths; residual intensities r (central values for the absorptions and peak values for the emissions), and the heliocentric radial velocities for the absorption cores or for the whole emissions. Residual intensities *r* are rounded to hundredths (0.01) and radial velocities V_r, to 1 km/s. The table contains only the data based on high-resolution spectra with the velocities controlled and corrected by telluric lines. The residual discrepancy of the zero points of the radial velocity scales for different observing dates does not exceed 0.6 km/s if estimated from interstellar NaI (1) lines.

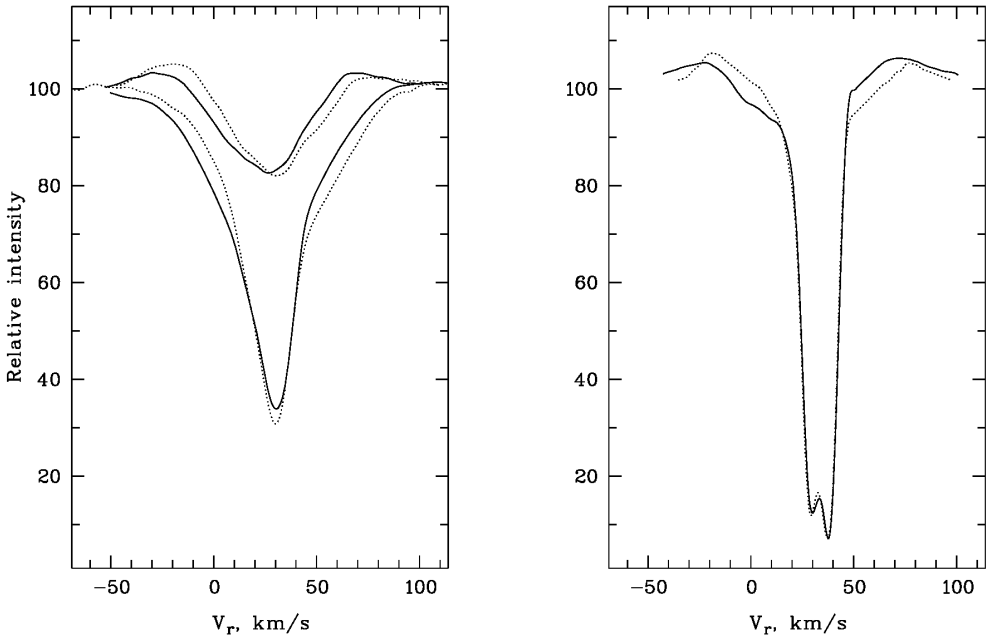

Fig. 6. Line profile variations in the spectrum of 3 Pup. The solid and dotted lines correspond to the spectra taken on December 25, 2004 and December 26, 2006, respectively. Left: FeII(48) 5363 Å (top) and averaged FeII(42) 4924, 5018 Å. Right: NaI(1) 5896 Å.

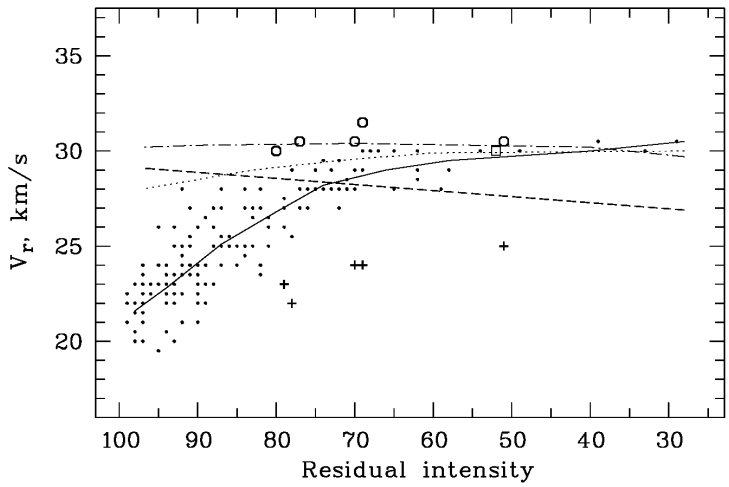

Fig. 7. Dependence of the radial velocity measured from the absorption core on its central intensity. The dots show individual absorptions of iron-group ions in the spectrum taken on December 25, 2004 and the solid line shows the $V_r(r)$ curve averaged over these absorptions. The mean $V_r(r)$ dependencies for the same group of absorptions are shown by: the dotted line (14.03.03), the dashed line (4.11.2008), and the dash-and-dot line (26.12.06 and 07.02.02). The Mg II and Si II lines are shown by the crosses (the spectrum of December 25, 2004), open circles (December 26, 2006), and the square (4.11.2008).

The top rows of Table 2 give the V_r values for NaI and other interstellar lines and bands. The uppermost row lists the velocities of the interstellar components of NaI (1) lines as a whole (i.e., averaged over all our measurements: 33.3f0.2 km/s). Below we list the velocities of the two components (one under another) in the cases where both can be discerned. The short-wavelength component with $V_r \approx 28$ km/s is stronger in KI (1) and CaII (1) lines and the long-wave component with $V_r \approx 37$ km/s, in NaI (1) lines. Note that the velocities of

diffuse interstellar bands (DIB) are determined from different sets of these bands because of the different operating wavelengths intervals.

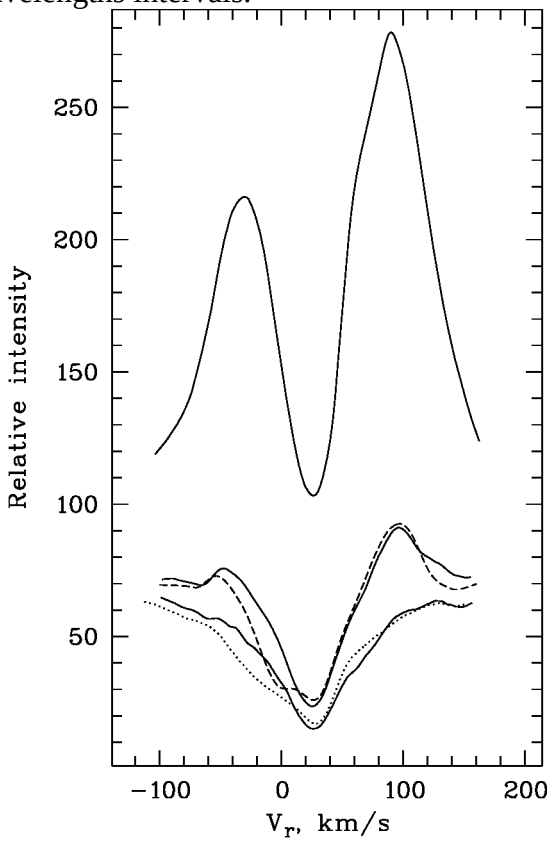

Fig. 8. Central parts of Balmer lines in the spectrum of 3 Pup taken on December 26, 2006. From top to bottom: Hα, Hβ, and Hγ. For comparison, the dashed and dotted lines show the spectrum of Hβ taken on November 4, 2008 and the spectrum of Hγ taken on April 125.12.04.

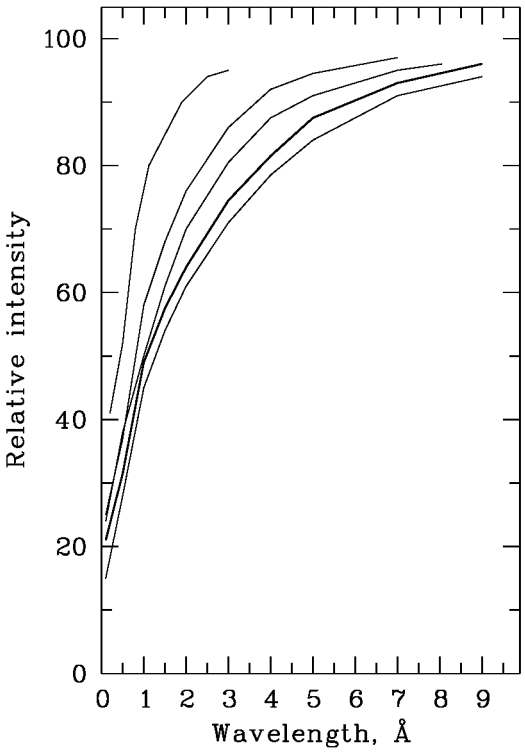

Fig. 9. Hγ half profiles in the spectra of 3 Pup (the thick line) and of the comparison stars (the thin lines, from top to bottom: 6 Cas (A3 Ia-0), α Cyg (A2 Ia), HD 13476 (A3 Iab), HD 210221 (A3 Ib).

Does the absorption depth correlate with the velocity measured from the same absorption? Figure 7 shows the $V_r(r)$ curves based on the data from Table 3. The strongest systematic trend of velocity with depth was observed on December 25, 2004. For this date the positions of individual lines are shown on the plot: the weakest FeII, TiII, CrII absorptions (bottom left), the FeII(42) triplet (top right), and MgII, SiII lines (below the iron-group lines). The vertical scatter of symbols gives an idea of the accuracy of velocity measurements based on lines of different intensity. For the dates with appreciably smaller velocity differences than on December 25, 2004 we show in Fig. 7 only the generalized $V_r(r)$ curves. The dependencies for 2006 and 2007, which are very close to each other, are shown by a single, almost horizontal line. We used the $V_r(r)$ curves in the generalization and averaging the radial velocity data and list the results in Table 2.

Our measurements suggest that the most stable feature is the outer shell of 3 Pup. Velocity variations with time are minimal, and the velocity values for forbidden emissions and sharp shell cores of FeII(42) absorptions and other strong iron-group ion lines are close to each other. The mean velocity averaged over the above lines (rows 9, 10 and 12–14 in Table 2, respectively) can be adopted as the systemic radial velocity for the system as a whole: V_{sys} = 28.5 + 0.5 km/s, which differs from both likely values of γ = 25.6 and 23.5 km/s implied by the model proposed by Plets et al. [3].

On the other hand, the weakest photospheric absorptions ($r \rightarrow 1$, row 16 in Table 2) show well-defined date-to-date velocity variations amounting to 7 km/s between December 25, 2004 and December 26, 2006. As is evident from a comparison of rows 15 and 16 of Table 2, stronger and photospheric MgII and SiII absorptions show similar velocities and similar velocity variations with time. The latter fact is immediately apparent even

for permitted lines (row 11 in Table 2), most of which are slightly blueshifted relative to weakening absorptions. These facts, like the narrowing of forbidden emissions compared to permitted emissions, are consistent with the interpretation of 3 Pup as a star with an equatorial disk and a low-mass companion [3]. Our V_r values for photo-spheric absorptions lie within the limits imposed by the radial velocity curve based on the data of Johnson and Neubauer [23], but our fragmentary observations are insufficient for its validation and correction.

The velocities of the absorption cores of the first Balmer series lines, except Hα, appear to be close to the velocities of strong FeII absorptions, i.e., to V_{sys}. The spectra taken on December 25, 2004 and December 26, 2006 show a small Balmer progress. More conclusive evidence for the radial gradient of velocity in the shell of 3 Pup is provided by the Hβ (November 4, 2008) and Hγ (December 25, 2004) profiles. These profiles exhibit not only the main cores used to infer the velocities V_r listed in Table 2, but also the blueshifted components with $V_r \approx 0$ km/s (see Fig. 8). The extra-atmospheric ultraviolet resonance lines are shifted with respect to the photospheric lines even more, by (–50... –60) km/s [10].

3.3. Spectral Type and Distance

The blue part of the spectrum of 3 Pup, where emission components of the lines are weak, resembles the corresponding regions in the spectra of A2–3 Ib-type stars, and, in particular, those of HD 207673 and BD +60 2542 (A2 Ib), HD 210221 (A3Ib), and HD 13476 (A3 Iab) as reported by Verdugo et al. [27, 28], who observed it with a resolution which is close to that of our spectra. Given that the profiles of metal lines suffer from distortions that increase with wavelength and line intensity, we performed quantitative classification by shallow Fe I, FeII, and TiII absorptions and by the Mg I and MgII lines in the 4280–4700 Å wavelength interval. The calibration relations of the equivalent width as a function of spectral type W(Sp) are based on the equivalent widths of A0–F0-type supergiants from [29]. In addition, we also compared the ratios of the central depths in the blue parts of the spectra of 3 Pup and η Leo A0 Ib, HD 21389 A0 Ia, α Cyg A2 Ia, HD 17378 A5 Ia determined using NES spectrograph. We estimated the luminosity class and Mv from the equivalent widths and profiles of Hδ and Hγ (we show the latter for 3 Pup and comparison stars in Fig. 9). We also estimated the luminosity from the equivalent width of the OI 7774 Å triplet (W = 1.42 Å, which corresponds to luminosity class Ib). Our final estimates of the spectral type and absolute magnitude of 3 Pup are A2.7 +0.3 Ib and Mv= $-5.5^m + 0.3^m$, respectively.

The trigonometric parallax of 3 Pup, which corresponds to d > 1.4 kpc, is too small (about 0.6.″) and therefore too uncertain. The distance estimates based on the Av(d) dependencies derived by Neckel and Klare [30] and Plets et al. [3] are equally unreliable. They indicate that interstellar extinction increases slowly with distance towards 3 Pup, and that it reaches $Av(3\ Pup) \approx 0.5^m$ at d ≈ 1.4 kpc, whereas both the stellar and nonstellar radial velocities of 3 Pup are observed already at 0.3–0.5 kpc. Currently, the most accurate results for 3 Pup are provided by the method of spectroscopic parallax, which yields d ≈ 0.7 kpc for the E(B–V) and Mv values mentioned above.

4. CONCLUSIONS

In the case of Fe II lines in the spectrum of 3 Pup there is an evident contribution of the shell, which gives the profiles their specific shapes: the wings are raised by emissions, whereas the core is sharpened. The latter is apparent even for the absorptions with R≈ 20 at λ > 4300 Å and becomes more pronounced with increasing line strength. Sharpened cores are typical of Balmer lines except for Hα.

The profiles of the CaII(2) triplet have a “two-step” shape: a narrow double peak is appreciably redshifted with respect to the relatively broader “pedestal”. The radial velocity of the peak is close to the velocities of forbidden emission lines, whereas that of the lower component of the profile is close to the velocities determined from the permitted emissions.

Line profiles vary with time: both the magnitude and the sign of the absorption asymmetry, and the blue-to-red emission intensity ratios vary from one spectrum to another. The profiles of all forbidden emissions in the

recorded region of the spectrum have the same shapes and widths and yield the same radial velocity within the errors.

Radial velocity variations of forbidden emissions and sharp envelope cores of FeII(42) absorptions and other strong iron-group ion lines are minimal and the velocities of these lines are close to each other. The mean velocity averaged over the above lines can be adopted as the radial velocity of the system as a whole: V_{sys} = 28.5 ± 0.5 km/s.

The weakest photospheric absorptions (with residual intensities $r \rightarrow 100$) and the photospheric absorptions Mg II, Si II exhibit bona fide day-to-day velocity variations amounting to 7 km/s.

Shallow Fe I, Fe II, and Ti II absorptions and Mg I, Mg II lines in the 4280–4700 Å wavelength interval yield a spectral type of A2.7 ±0.3 Ib. The equivalent widths and profiles of Hδ and Hγ, and the equivalent width of the OI 7774 Å triplet yield an absolute magnitude of Mv= $-5.5^m \pm 0.3^m$.

Table 3. Residual intensities r and heliocentric radial velocities $V_\odot$ for individual lines in the high-resolution spectra of 3 Pup, taken on different dates. The complete electronic version of this table is available at `www.sao.ru/hq/ssl/3Pup-lines.ps` and `www.sao.ru/hq/ssl/3Pup/Table3.html`.

Element	λ, Å	14.03.03		25.12.04		26.12.06		07.02.07		04.11.08	
		r	$V_\odot$, km/s	r	$V_\odot$, km/s	r	$V_\odot$, km/s	r	$V_\odot$, km/s	r	$V_\odot$, km/s
[FeII]19F	5158.78			1.05	27	1.02	26	1.05	29	1.06	26
MgI(2)	5167.33	0.90	29			0.94	33			0.94	30
FeII(42)	5169.03	0.29	30	0.27	31	0.23	30	0.25	29	0.27	27
MgI(2)	5172.69			0.87	26	0.88	33	0.88	33	0.86	32
FeII	5177.39			0.97	25			0.98	29	0.98	27
FeII	5180.32									0.98	30
MgI(2)	5183.61	0.84	27	0.85	25	0.86	29	0.86	30	0.86	30
TiII(86)	5185.91	0.90	25	0.93	23	0.92	28	0.93	27	0.92	29
TiII(70)	5188.69	0.89	28	0.88	26	0.89	30	0.89	30	0.89	29
FeII(49)	5197.58	0.69	30	0.78	29	0.73	30	0.74	30	0.74	26
CrI(7)	5208.43							0.97	30	0.98	32
FeII(49)	5234.62	0.73	30	0.74	30	0.69	30	0.72	30	0.72	27
CrII(43)	5237.32	0.86	30			0.84	30	0.85	31	0.85	29
ScII(26)	5239.82			0.97	24	0.98	28	0.97	29	0.97	30

Table 3. (Contd.)

Element	λ, Å	14.03.03		25.12.04		26.12.06		07.02.07		04.11.08	
		r	$V_\odot$, km/s	r	$V_\odot$, km/s	r	$V_\odot$, km/s	r	$V_\odot$, km/s	r	$V_\odot$, km/s
CrII(38)	5243.50									0.98	26
CrII(23)	5249.43					0.98	29			0.98	30
FeII(49)	5254.93	0.93	28	0.92	27	0.91	30	0.92	30	0.92	29
FeII	5260.26	0.94	27	0.93	23			0.92	32	0.93	28
FeII(48)	5264.80	0.88	26					0.87	27	0.87	25
FeII(49)	5276.00	0.70	30	0.72	30			0.71	30	0.72	26
CrII(43)	5279.95							0.94	30	0.94	28
FeII(41)	5284.10	0.90	29	0.90	27	0.90	31	0.89	30	0.90	29
FeII	5291.67	0.97	29	0.97	24	0.97	29	0.96	30	0.97	27
CrII(24)	5305.86							0.94	29		

CrII(43)	5308.42	0.95	30	0.95	24	0.94	31	0.95	31	0.95	30
CrII(43)	5310.69			0.97	22			0.96	30	0.98	28
CrII(43)	5313.58	0.93	29	0.92	24	0.90	30	0.90	30	0.92	28
FeII(49)	5316.66	0.62	29	0.63	28	0.60	28	0.59	28	0.60	24
FeII(49)	5325.56	0.90	29	0.91	24	0.91	30	0.91	31	0.90	27
[FeII]19F	5333.65	1.03	26	1.02	26	1.03	22	1.04	27	1.01	24
CrII(43)	5334.87	0.94	31	0.93	24	0.93	31	0.93	29	0.92	27
FeII	5339.59			0.96	26	0.96	32	0.97	32	0.96	31
FeII(48)	5362.87	0.84	30	0.83	27	0.82	30	0.82	30	0.82	26
FeI(15)	5371.49					1.03	30	1.02	31	1.04	31
TiII(69)	5381.03	1.04	27	1.03	24	1.03	27	0.97	25	1.03	26
FeI(1146)	5383.38	0.99	31					0.98	25	0.98	29
FeII	5387.07	0.97	32	0.97	24			0.98	31	0.97	28
FeII	5395.86	0.98	28					0.98	29	0.98	29
CrII(23)	5407.62							0.98	31	0.97	30
FeII(48)	5414.07					0.93	30	0.95	32		
TiII(69)	5418.78	0.99	27					0.97	30		
CrII(23)	5420.93							0.97	31	0.97	29
FeII(49)	5425.25	0.93	28	0.93	25	0.92	28	0.92	29	0.93	26
FeII	5427.82							0.97	30	0.98	29
FeII(55)	5432.98	0.95	27			0.95	28	0.95	26	0.95	25
FeII	5439.71									0.99	27
FeI(15)	5446.91					1.02	33	1.03	31	1.03	30

Table 3. (Contd.)

Element	λ, Å	14.03.03		25.12.04		26.12.06		07.02.07		04.11.08	
		r	$V_\odot$, km/s	r	$V_\odot$, km/s	r	$V_\odot$, km/s	r	$V_\odot$, km/s	r	$V_\odot$, km/s
FeI(15)	5455.61	1.03	29	1.02	26	1.03	27	1.02	27	1.03	29
CrII(50)	5478.37	0.94	30	0.95	23	0.95	31	0.95	30	0.95	28
FeII	5482.31	0.97	24					0.96	29		
FeII	5487.63	0.97	27					0.97	30	0.98	28
CrII(50)	5508.62	0.96	27					0.96	27	0.97	25
CrII(23)	5510.71									0.97	29
ScII(31)	5526.81	1.05	28			1.04	27	1.03	30	1.05	29
FeII(55)	5534.84	0.88	29	0.87	28	0.87	30	0.86	31	0.87	27
FeII(166)	5544.76									0.97	29
FeI(686)	5615.64							0.98	31		
CrII(189)	5620.63									0.99	30
FeII(57)	5627.49			0.99	22	0.99	28	0.98	29	0.99	30
FeII(57)	5657.92			0.97	26	0.98	32	0.97	30	0.97	33
ScII(29)	5684.19									1.02	27
FeII(164)	5747.90			0.99	22					0.99	26
DIB	5780.37	0.95	27	0.93	26	0.93	26	0.94	31	0.94	27

DIB	5793.22			0.99	23						
FeII(211)	5795.87			0.99	22						
DIB	5796.96	0.97	38	0.96	35	0.97	33	0.97	34	0.97	36
FeII(163)	5813.67	0.97	30	0.98	20			0.98	25	0.98	25
FeII(164)	5823.15			0.99	23	0.99	26			0.99	26
FeII(182)	5835.49					0.99	33			0.99	28
DIB	5849.80	0.98	35	0.99	31			0.99	31	0.98	30
HeI (11)	5875.72	0.96	30	0.96	24	0.96	26	0.95	30	0.96	31
NaI (1)	5889.95	0.06	33	0.03	33	0.04	33	0.07	33	0.08	33
NaI (1)	5895.92	0.10	33	0.07	34	0.08	33	0.13	34	0.14	33
SiII(4)	5978.93	0.94	28			0.93	31	0.93	32		
FeII(46)	5991.37	1.07	26	1.06	26	1.07	28	1.07	29		
CrII(105)	6053.46			0.99	22						
FeII	6060.99			0.99	19						
FeII(46)	6084.10	1.03	26	1.03	25	1.04	26				
NiI (45)	6108.12	1.01	28								
FeII(46)	6113.32	0.98	27	0.98	22	0.98	30				

Table 3. (Contd.)

Element	λ, Å	14.03.03		25.12.04		26.12.06		07.02.07		04.11.08	
		r	$V_\odot$, km/s	r	$V_\odot$, km/s	r	$V_\odot$, km/s	r	$V_\odot$, km/s	r	$V_\odot$, km/s
CaI (3)	6122.22			0.99	25						
BaII(2)	6141.73			0.99	21	0.99	29				
FeII(74)	6147.74	0.93	27	0.92	24	0.92	28				
FeII(74)	6149.25	0.93	30	0.93	28	0.93	31				
CaI(3)	6162.18			1.02	24						
FeII(200)	6175.16	0.98	29	0.97	23						
FeII(163)	6179.39	0.99	28	0.98	22						
DIB	6195.96	0.98	31	0.98	32	0.97	27				
FeI(62)	6219.29	1.01	27								
FeII(74)	6238.39	0.94	27	0.94	23	0.93	27				
FeII(74)	6247.55	0.88	29	0.87	27	0.85	31				
DIB	6283.85			0.92	34						
[OI]1F	6300.30	1.14	26	1.12	28	1.12	29				
FeII	6317.99					0.95	31				
FeII(199)	6331.96	0.98	30			0.98	30				
FeI(62)	6335.34	1.01	29								
SiII(2)	6347.10	0.70	32	0.69	24	0.70	31				
FeI(13)	6358.70	1.01	30	1.02	27	1.02	27				
[OI]1F	6363.78	1.06	28	1.05	28	1.04	28				
SiII(2)	6371.36	0.76	33	0.76	25	0.77	31				
DIB	6375.95			0.99	31						
DIB	6379.29	0.98	30	0.98	30	0.99	27				
FeII	6383.72			0.98	25						
FeI(168)	6393.61			1.01	26						
FeII(74)	6416.93	1.06	26	0.94	24	1.05	26				
FeII(40)	6432.68	1.15	24			1.14	24				
FeII	6442.95			0.98	27						
FeII(199)	6446.41	0.98	25	0.97	26	0.98	31				
FeII(74)	6456.38	0.81	30			0.80	31				

REFERENCES

1. D. Hoffleit and C. Jaschek, The Bright Star Catalogue (Yale University Observatory, New Hawen USA, 1982).
2. I. Jr. Iben and A. V. Tutukov, Astrophys. J. 418, 343 (1993).
3. H. Plets, C. Waelkens, and N. R. Trams, Astronom. and Astrophys. 293, 363 (1995).
4. M. P. Fitzgerald, Astronom. and Astrophys. 4, 234 (1970).
5. van F. Leeuwen, Astronom. and Astrophys. 474, 653 (2007).
6. A. J. Cannon, Ann. Astr. Obs. Harvard Col. 28, 131 (1901).
7. A. C. Maury, Ann. Astr. Obs. Harvard Col. 28, 1 (1987).
8. P. W. Merrill, Publ. Astronom. Soc. Pacific 46, 156 (1934)
9. C. S. Beals, Publ. Dom. Astrophys. Obs. Victoria 9, 1(1951).
10. A. C. Rovero and A. E. Ringuelet, Monthly Notices Roy. Astronom. Soc. 266, 203 (1994).
11. W. A. Hiltner, Astrophys. J. 105, 212 (1947).
12. A. C. Danks and M. Dennerfeld, Publ. Astronom. Soc. Pacific 106, 382 (1994).
13. P. Swings, Annales d'Astrophys. 13, 114 (1950).
14. D. Crespin and J. W. Swensson, Bull. Acad. Roy. Belgigue, d. sc. 38, 376 (1952).
15. W. W. Morgan, H. A. Abt, and J. W. Tapscott, Revised MK spectral atlas for stars earlier than the Sun (Yerkes Obs., Univ. of Chicago and Kitt Peak Obs., 1978).
16. V. Panchuk, V. Klochkova, M. Yushkin and I. Najdenov, in The UV Universe: stars from birth to death, Proceedings of the Joint Discussion No. 4 during the
IAU General Assembly of 2006, Ed. by A. I. Gomez de Castro and M. A. Barstow. (Editorial Complutense, Madrid, 2007), p. 179.
17. V. E. Panchuk, V. G. Klochkova, M. V. Yushkin, I. D. Naidenov, Opticheskii Zhurn. 76, 42 (2009).
18. V. E. Panchuk, J. D. Najdenov, V. G. Klochkova, et al., Bull. Spec. Astrophys. Obs. 44, 127 (1998).
19. M. V. Yushkin, V. G. Klochkova, Preprint of the Special Astrophysical Observatory No 206 (Nizhnii Arkhyz, Special Astrophysical Observatory of the Russian Academy of Sciences, 2005).
20. N. Manset and J.-F. Donati, Proc. of the SPIE 4843, 425(2003).
21. R. G. Tull, P. J. MacQueen, C. Sneden, and D. L. Lambert, Publ. Astronom. Soc. Pacific 107, 251 (1995).
22. V. G. Klochkova, V. E. Panchuk, M. V. Yushkin, and D. S. Nasonov, Bull. Spec. Astrophys. Obs. 63, 386, (2008).
23. H. L. Johnson and F. J. Neubauer, Publ. Astronom. Soc. Pacific 58, 248 (1946).
24. D. Pourbaix, A. A. Tokovinin, A. H. Batten, et al., Astronom. and Astrophys. 424, 727 (2004).
25. L. O. Loden, The Messenger No. 68, 26 (1992).
26. L. O. Loden and A. Sundman, Astronom. and Astrophys. Suppl. Ser. 112, 9 (1995).
27. E. Verdugo, A. Talavera, and A. I. Gomez de Castro, Astronom. and Astrophys. Suppl. Ser. 137, 351 (1999).
28. E. Verdugo, A. Talavera, and A. I. Gomez de Castro, Astronom. and Astrophys. 346, 819 (1999).
29. K. Venn, Astrophys. J. Suppl. 99, 659 (1995).
30. Th. Neckel and G. Klare, Astronom. and Astrophys. Suppl. Ser. 42, 251 (1980).